Progress In Electromagnetics Research C, Vol. 111, 173–189, 2021

Design of a 3-Port Compact MIMO Antenna Based on Characteristics Mode Analysis Approach

Asutosh Mohanty[1, *] and Bikash R. Behera[2]

Abstract—In this paper, a 3-port compact MIMO antenna is designed using Characteristics Mode Analysis (CMA). It consists of three antenna elements. Ant-1 is 45° tilted, and Ant-2 and Ant-3 have L-bend transitions. Ant-2 is 1/4th, and Ant-3 is 1/2 in size w.r.t. Ant-1. To improve 10-dB impedance bandwidth and isolation > 17 dB, fractal slot is etched at bottom, and deformity in antenna structures has three distinct modes. Ant-1 operates in UWB mode from (4.8–10.6) GHz with 75.32% IBW, and Ant-2 and Ant-3 operate in wide-band mode from (8.1–10.8) GHz with 28.57% IBW and from (7.2–9.8) GHz with 30.58% IBW. CMA is utilized to investigate the anonymous behaviour of antenna, predicts modal significance (MS), characteristics angle (CA), and eigen values (EV). From these parameters, bandwidth potential, radiation energy source, and Q-factor are estimated. For investigations, first six modes are swept in modal navigator, where dominant modes are traced as ideal antenna resonant modes, and unwanted modes are neglected. The antenna gain is (3–7) dBi with ECC < 0.08. The proposed antenna is fabricated and measured for validation. From the outcomes, it is found suitable for UWB, air traffic, and defense tracking, meteorological, amateur satellite, maritime vessel traffic controlling, and X-band satellite applications.

1. INTRODUCTION

Multiple-input-multiple-output (MIMO) antenna technology today embraces advanced wireless communications since multi-users can be served with same frequency and time [1, 2]. Due to wide range of advantages in MIMO technology such as increased spectral efficiency, high range data capacity, high data rate, and low operating cost, it forms a core network performance stability in antenna technology [3, 4]. Since MIMO system requires an array of antenna elements, from design perspective it requires precision of antenna locations to minimize near-field coupling and enhance isolation [5]. There are various techniques adopting orienting antenna elements for radiation diversity and decoupling elements in MIMO configurations.

Crossed printed circuit boards with dipoles are adopted in [6] for orthogonal polarization. A cavity slot integrated antenna design with polarized E-fields is implemented in [7] for diversity. Isolation decoupling networks are provided at antenna feed lines in [8]. Utilizing stub elements as isolator [9], T-slots as radiator with neutralization line as isolator [10] are implemented to provide pattern diversity. Introducing separate Tx and Rx monopole antennas in a hand held PCB, both isolation and diversity are achieved [11]. Integration of printed dipoles with chamfered slot provides dual-polarization diversity in [12]. Mutually decoupling modes and near-degenerate modes using rectangular DRA minimize the mutual spatial overlapping of E-field magnitudes of antenna elements technique adopted by [13]. Reactively loading dummy elements with different impedances provides simple and efficient decoupling technique for MIMO antenna in [14]. Employing a ring loaded with periodical interdigital capacitors

Received 20 January 2021, Accepted 31 March 2021, Scheduled 6 April 2021
* Corresponding author: Asutosh Mohanty (asutoshmohanty.kiit0409@gmail.com).
[1] School of Electronics Engineering, KIIT Deemed University Bhubaneswar, Odisha 751024, India. [2] Advanced RF and Microwave Lab, Department of Electronics and Telecommunication Engineering, IIIT Bhubaneswar, Odisha 751003, India.

for selective excitation to achieve polarization and patterns diversity MIMO antenna is adopted in [15]. A pattern diversity MIMO antenna with a Fabry-Perot cavity (FPC) using partially reflective surface (PRS) for ceiling-mounted WLAN access points is designed by [16]. Implementing MIMO isolation element as radiator for laptop computers is designed in [17].

The reported article provides insight into 3-port MIMO antenna design configurations with distinctive characteristics observed primarily in radiation diversity and isolation improvements. Since modern MIMO antenna demands highly compact, hand-held driven portable devices for Personal Area Networks (PAN), device integrable and performance centric attributes, to achieve a compact MIMO antenna module, the classical approach of CMA is firstly studied and implemented in our proposed antenna. The theory reveals discrimination of ideal and non-ideal modes for antenna resonance mechanism, bandwidth potential, radiation energy type, and Q-factor. The main highlights of proposed antenna design are:

- The proposed MIMO design intuition is to assist a compact antenna with spatial and pattern diversity. Hence, the antenna design system constitutes three distinct antennas with different orientations, whose electrical lengths are also different, aiming to operate in different frequency operational modes without any supplementary isolation network. In order to assemble 3-port antenna elements in a compact space, metallic wavering properties like scaling, compression, translation, and contraction are invoked. Since no decoupling network is provided and at the same time to assert good impedance matching at 3-ports with a connected ground topology, antenna elements are aligned with 45° metallic contortions with fractal slot ground geometry. The metallic contortions in antennas act like an impedance matching transformer [20].
- Ant-1 is operated in wideband mode, and Ant-2 and Ant-3 operate in narrow band modes. Each antenna element is primarily differentiated, aiming to provide low mutual correlation and independent frequency of operation. Ant-1 can be used in UWB, civil and military radar applications. Ant-2 can be distinctively used as meteorological, amateur satellite, maritime vessel traffic controlling, and X-band satellite applications. Ant-3 can be used for Wi-Fi-6E, military, and weather radars.
- The proposed antenna is a type of multi-antenna system with different frequencies of applications assisting spatial and pattern diversity but consistent to the fundamental integral principles of MIMO technology. According to authors' knowledge, no research articles till now has discussed CMA implementation for a 3-port MIMO antenna with distinctive modal attributes.

2. THEORY OF CHARACTERISTICS MODE ANALYSIS

The CMA theory was originally proposed by Garbacz (1965) for generalized modal expansion for antennas resonance and scattering fields [18]. Later Harrigton and Mautz (1971) developed characteristics mode theory for different conducting bodies [19]. Through CMA three main modal metrics can be found which are classified as [20–22]:

(i) Modal Significance (MS): It represents the maximum modal magnitude. MS = 1 represents perfect resonance condition. An MS value of $0.707 \approx 1/\sqrt{2}$ cross-overs signifies bandwidth potential. Mathematically it can be represented as:

$$\mathrm{MS}_n = \frac{1}{|1 + j\lambda_n|} \tag{1}$$

(ii) Characteristics angle (CA): It signifies an antenna at resonance when $\beta_n = 180°$. The sharp cross-overs at 180° shows that the antenna is at resonance, and the cross-over point is taken as ideal resonating mode.

$$\beta_n = 180° \left(1 - \frac{1}{\pi}\mathrm{arc}\left(\tan\left(\lambda_n\right)\right)\right) \tag{2}$$

(iii) Eigen values (EV): It signifies the type of modal energy stored. If $\lambda_n = 1$, the antenna is at resonance; if $\lambda_n < 1$, it has dominant capacitive energy/stored electric energy; if $\lambda_n > 1$, it has dominant inductive energy/stored magnetic energy.

3. CMA PERFORMANCE STUDY AND ANALYSIS ON ANTENNA STRUCTURES

Figure 1 shows the 3-port MIMO antenna geometry with optimized dimensions in millimeters. It consists of three antenna elements Ant-1, Ant-2, and Ant-3, where Ant-2 is 1/4th, and Ant-3 is 1/2 in size w.r.t. Ant-1 as shown in Figure 1(a). Ant-1 is 45° tilted which operates in UWB mode, and Ant-2 and Ant-3 have L-shaped structures (looks like mirror image w.r.t. one another) and operate in wide-band mode. The feeding locations of antenna elements are shown in red dots. Figure 1(b) shows the ground structure which consists of modified and truncated fractal slots (Koch curve) [25, 26]. The significance of antenna design elements is validated using CMA and characterized below. To begin CMA investigation, we have used CST microwave studio EM solver for analysis, extraction of modal parameters, and modal radiation patterns.

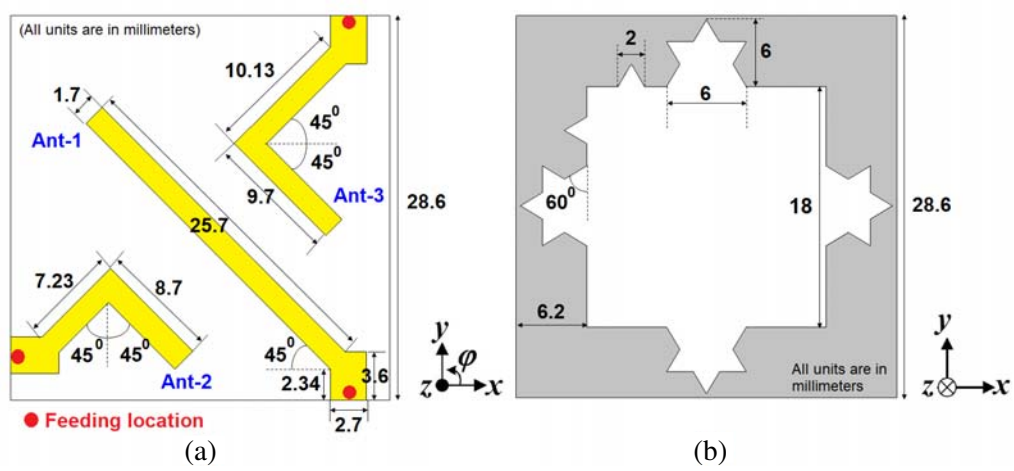

Figure 1. Proposed 3-port MIMO antenna geometry. (a) Top-view. (b) Bottom-view.

3.1. Effect of Normal Ground and a Fractal Slot Ground

Firstly, CMA with normal ground and fractal slot ground configurations are investigated. The modal currents and modal patterns with normal ground plane and fractal slot in ground are shown in Figure 2

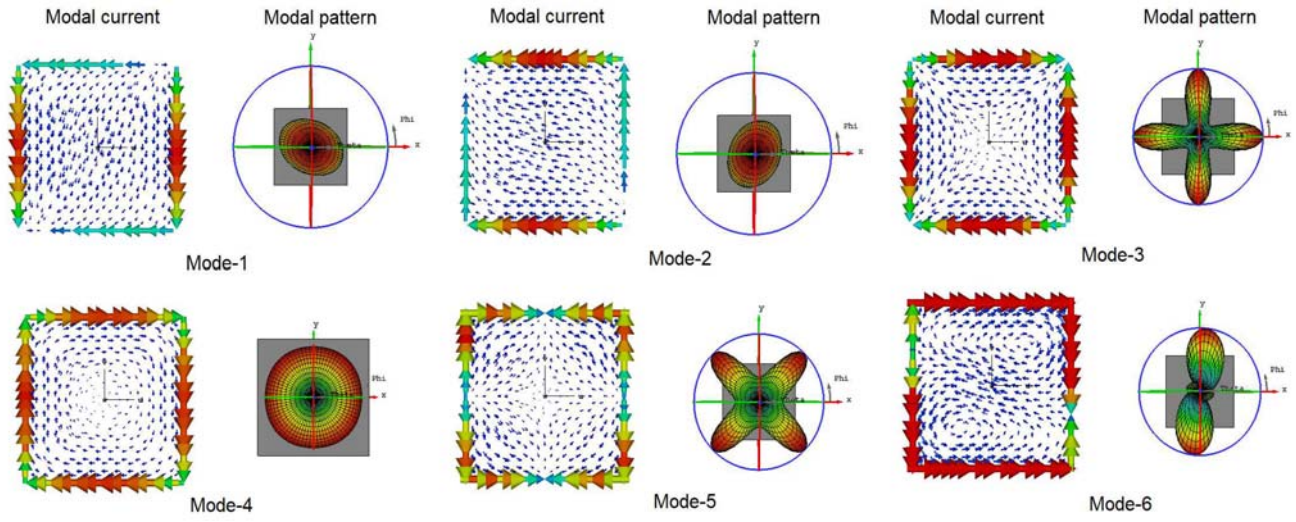

Figure 2. Modal currents and modal patterns for Mode-1 to Mode-6 for normal ground plane.

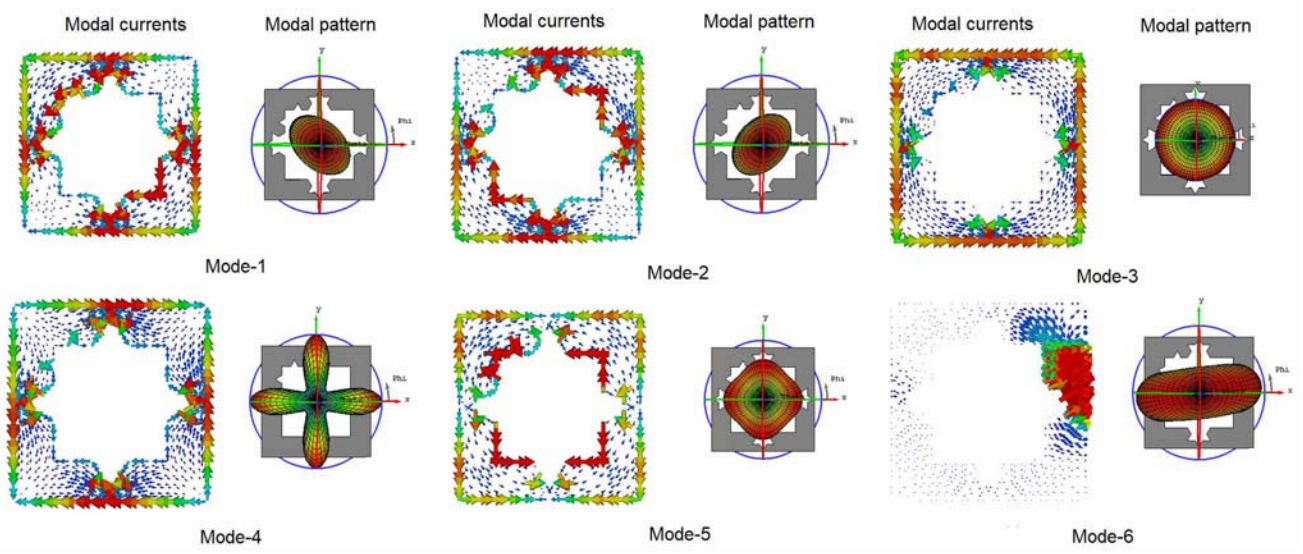

Figure 3. Modal currents and modal patterns for Mode-1 to Mode-6 for fractal slot ground plane.

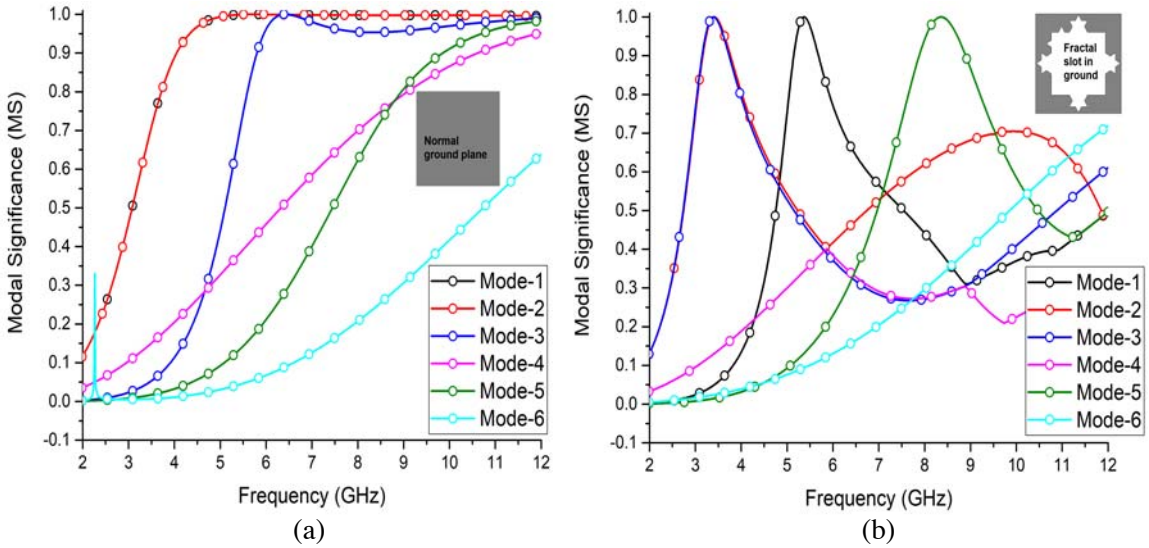

Figure 4. Modal significance for (a) normal ground plane, (b) fractal slot ground plane.

and Figure 3 for Mode-1 to Mode-6. The MS of normal ground plane is shown in Figure 4(a). From Figure 4, it is observed that fractal slots in ground has multi narrow band resonances as compared to normal ground. This is because the increased electrical length of fractal structure generates multiple-resonances. Mode-1 and Mode-2 are equal for both ground structures from modal currents and patterns. Mode-3/Mode-4 of normal ground is the same as Mode-4/Mode-3 of fractal slot ground (Mode-3 for fractal slot ground and Mode-4 of normal ground are inductive modes due to magnetic loops, hence are unwanted modes). Mode-5 and Mode-6 of normal ground are not considered, since Mode-5 fails to attain maximum MS while Mode-6 has dual magnetic loops. Mode-1, 2, 3, and 5 in fractal slot ground are considered as ideal modes as they have maximum MS, as shown in Figure 4(b). These modes have sharp Q-factors due to narrow multi-bands and contribute to antenna resonance.

3.2. Characteristics Mode Analysis of Ant-1 Configuration

Figure 5(a) shows the geometry of Ant-1 with fractal slot ground, and Figure 5(b) shows the MS. Since Ant-1 operates in UWB mode, it is observed that Mode-1 has magnitude > 0.707 confirming a UWB response. The resonant points at 5.32 GHz and 10 GHz coincide with S-magnitudes at corresponding points. Due to UWB behaviour, modal patterns are quad-directional, and the antenna has low Q-factor with wide bandwidth potential. Mode-2 and Mode-3 are also significant modes with MS = 1 but they are beyond the frequency-of-interest. Mode-4 has an inductive source with magnetic non-resonant loop mode. Mode-5 and Mode-6 are non-ideal modes since they fail to attain maximum MS magnitude as clearly observed from Figure 6.

Figures 7(a) and 7(b) show the characteristics angle and eigen values. From observation, Mode-1, Mode-2, and Mode-3 are at resonance due to sharp cross-over at $\beta_n = 180°$, hence they are classified as resonant modes. While Mode-4, Mode-5, and Mode-6 have dominant magnetic loop modes with range $90° < \beta_n < 180°$, hence they are classified as non-resonant modes.

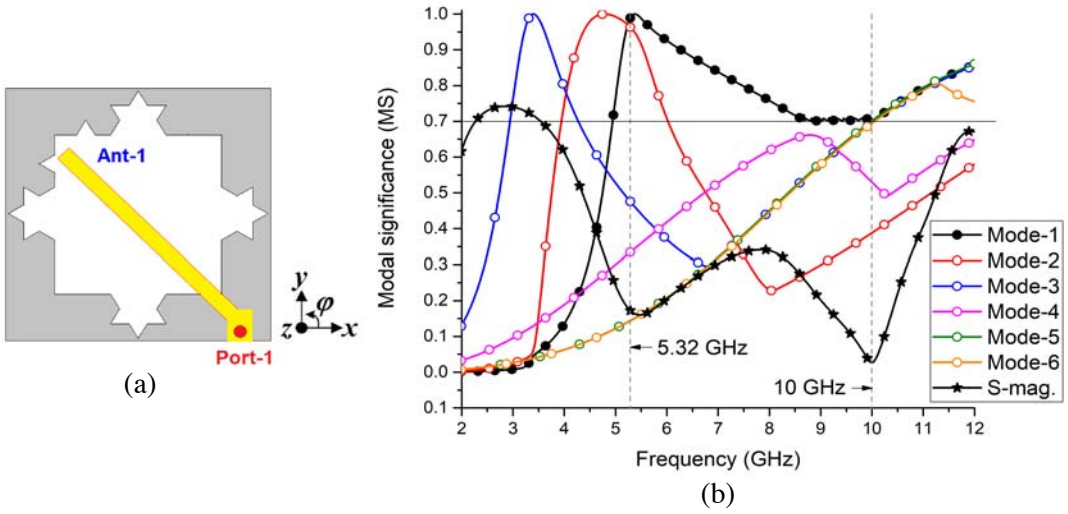

Figure 5. (a) Geometry of Ant-1 and fractal slot ground. (b) Modal significance (MS).

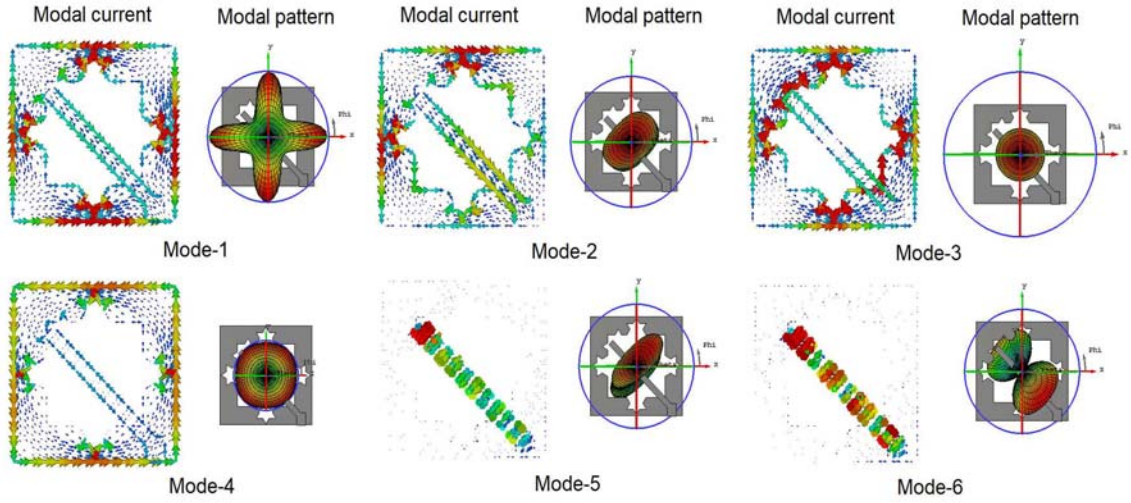

Figure 6. Modal currents and modal patterns for Mode-1 to Mode-6 for Ant-1 configuration.

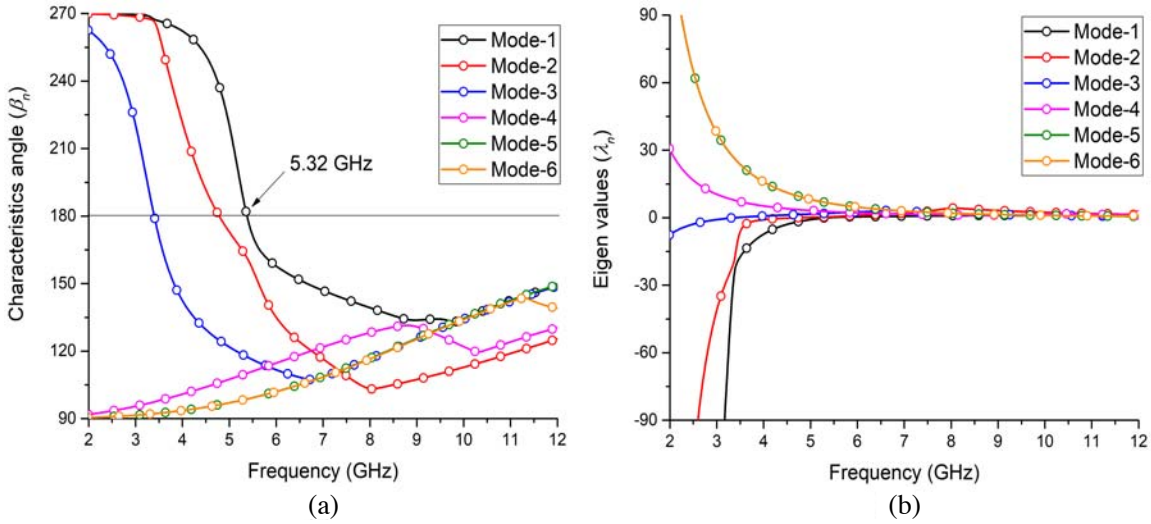

Figure 7. (a) Characteristics angle (β_n). (b) Eigen values (λ_n).

3.3. Characteristics Mode Analysis of Ant-2 Configuration

Figure 8(a) shows the geometry of Ant-2 and fractal slot with corresponding MS for Mode-1 to Mode-6 shown in Figure 8(b).

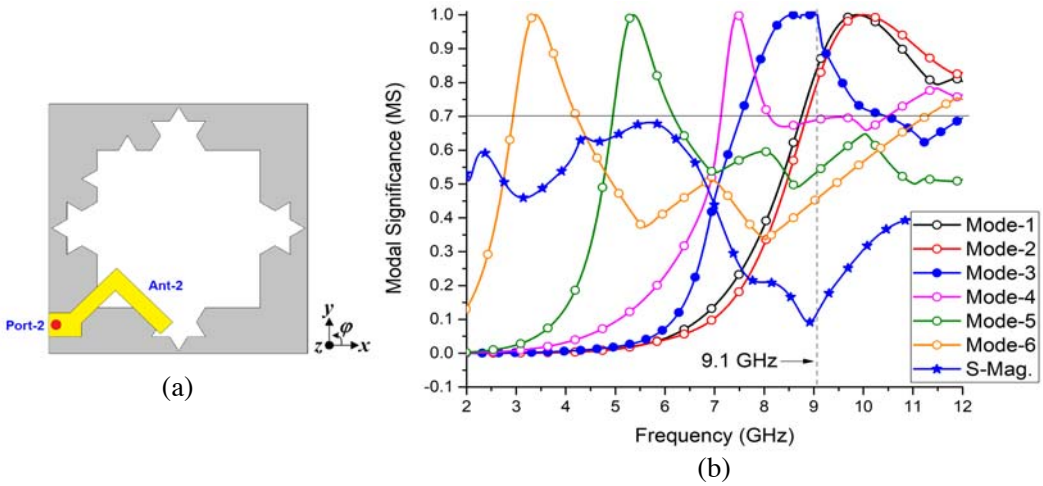

Figure 8. (a) Geometry of Ant-2 and fractal slot ground. (b) Modal significance (MS).

It is observed that all modes from Mode-1 to Mode-6 have maximum MS magnitudes, so now we have to categorize ideal modes and non-ideal modes. From Figure 10(a), it is confirmed that all modes are at resonance, and Figure 10(b) shows capacitively coupled modes with dominant stored electric field energy. Now left with us is the investigation of modal currents. It is observed from Figure 9 that Mode-1 to Mode-4 have symmetric radiations due to orientation of radiator in reference to fractal slot ground. However, Mode-4 has anticlockwise rotations and does not show any inductance effects due to nonhomogeneous magnetic loops in ground. Mode-5 and Mode-6 are non-radiating type structures since modal current density is spurious with nonuniform radiations. So Mode-3 is considered the fittest amongst all other modes as MS magnitudes with S-mag are in the resonant region of convergence. Ideal mode of Ant-2 has a sharp Q-factor/lower bandwidth than ideal mode in Ant-1.

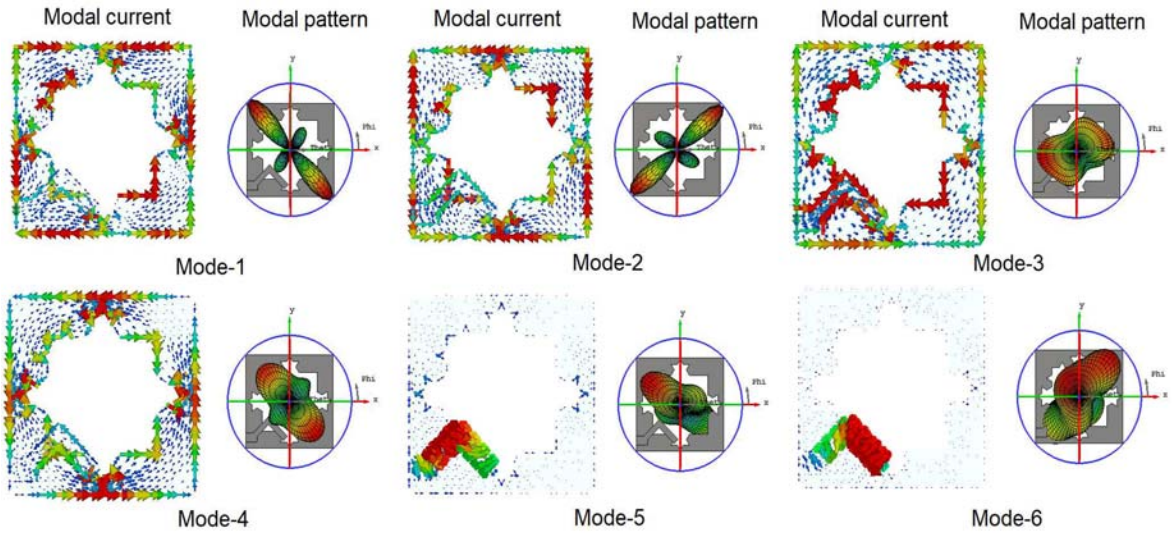

Figure 9. Modal currents and modal patterns for Mode-1 to Mode-6 for Ant-2 configuration.

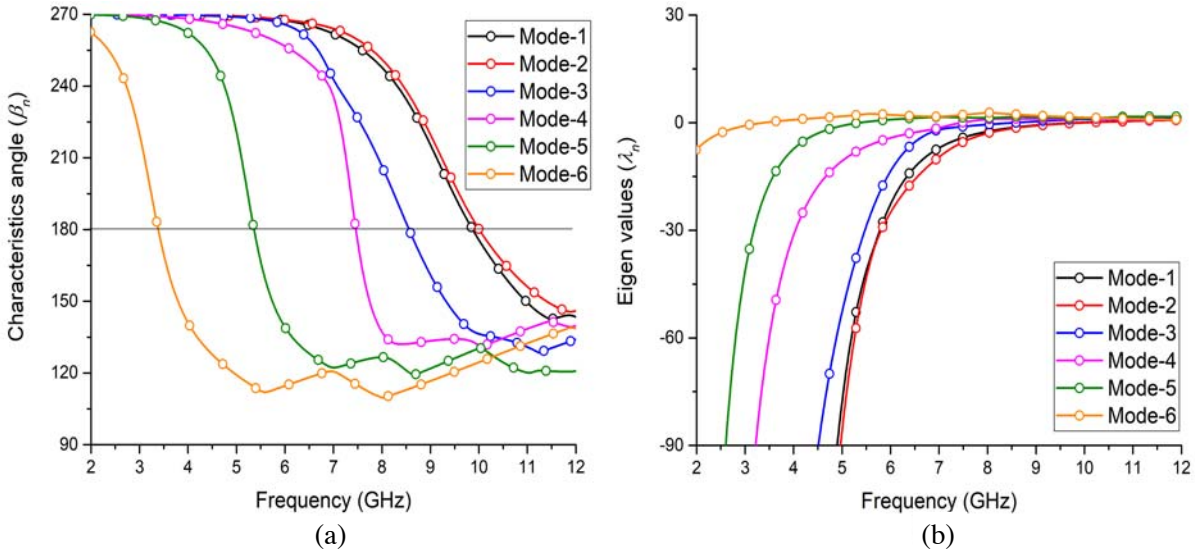

Figure 10. (a) Characteristics angle (β_n). (b) Eigen values (λ_n).

3.4. Characteristics Mode Analysis of Ant-3 Configuration

Figure 11(a) shows the geometry of Ant-3, and the corresponding MSs for Mode-1 to Mode-6 are shown in Figure 11(b). From modal observations, Mode-1 to Mode-5 have magnitude MS = 1, where Mode-1 has low Q-factor/wide bandwidth compared to all other modes. Mode-3 and Mode-5 do not exist in the band-of-interest, hence are discarded. Mode-6 is non-ideal mode, since it fails to attain maximum MS magnitude. To more vividly analyze, Figure 12 shows the modal currents with patterns, and Figures 13(a) and 13(b) show CA and EV performances. It is observed that all modes are at resonance except Mode-6, since CA ranges between $90° < \beta_n < 180°$ and $\lambda_n > 0$ showing the inductive characteristics for non-resonant type. The modal current for Mode-6 also shows spurious distributions of non-radiating currents. Hence, Mode-1 is considered as the ideal mode for Ant-3 since MS and S-mag are perfectly matched.

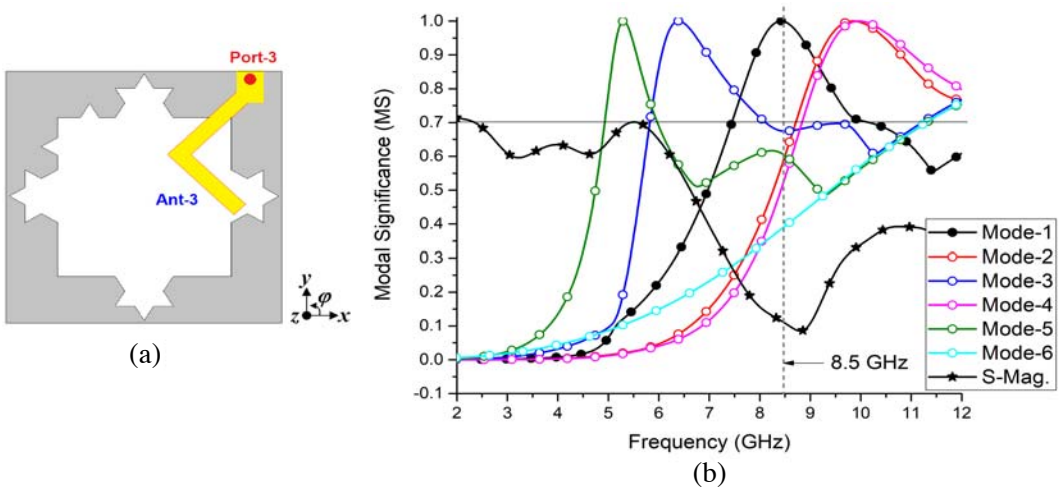

Figure 11. (a) Geometry of Ant-3 and fractal slot ground. (b) Modal significance (MS).

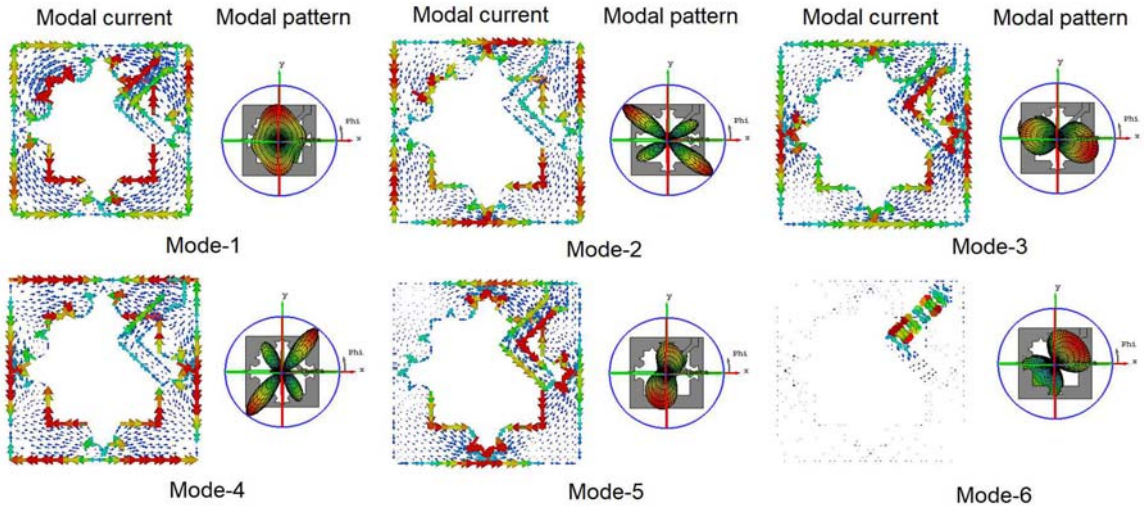

Figure 12. Modal currents and modal patterns for Mode-1 to Mode-6 for Ant-3 configuration.

3.5. Characteristics Mode Analysis of Integrated Antenna Geometry

We finally perform CMA on the integrated antenna geometry consisting of all antenna elements (Ant-1, Ant-2, Ant-3, and ground structure) as shown in Figure 14(a), and the corresponding dominant modal magnitudes plots at resonance are shown in Figure 14(b). The modal currents and modal patterns for antenna elements at dominant resonance are shown in Figure 15 for brevity. Figure 16(a) shows the CA plots of each antenna element, and Figure 16(b) shows the EV plots at aforementioned resonance cross-over points. Hence, the modal magnitudes are in good correlation with the CA and EV predicted cross-over points. Also, each antenna element exhibits a distinctive modal pattern. From the above analysis, we tabulate the modal performances for corresponding antenna geometries in Table 1. The ideal modes are best suited as antenna resonance modes and are differentiated in modal metrics compared to other significant modes. The ideal modes are investigated on MS, CA, and EV, which give insight on the antenna bandwidth potential, Q-factor, radiative energy type, and dominant energy stored. These modes have distinctive modal currents symmetry compared to non-ideal types. CMA also predicts the nature of energy distributions coupled over random conducting surface.

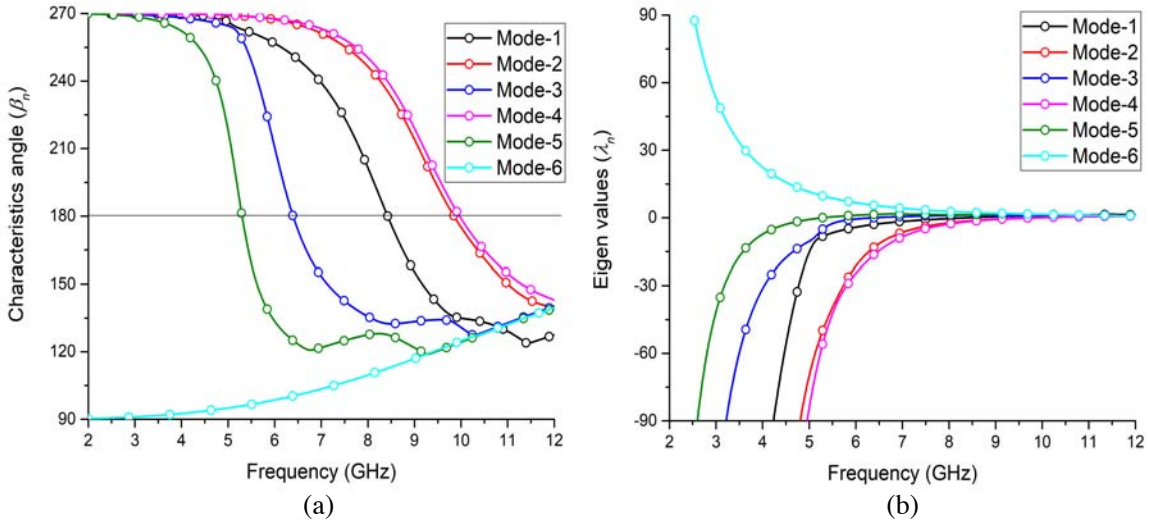

Figure 13. (a) Characteristics angle (β_n). (b) Eigen values (λ_n).

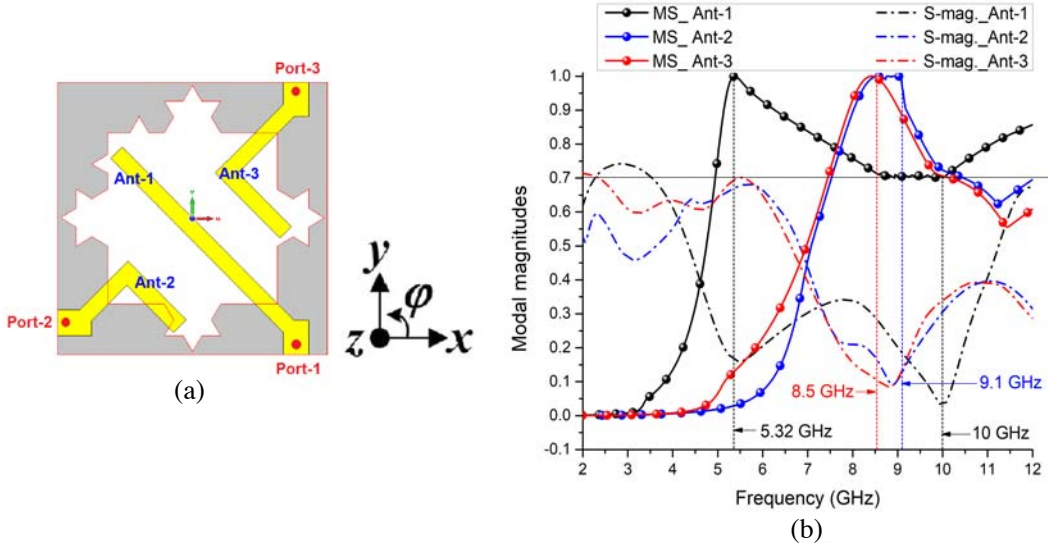

Figure 14. (a) Integrated antenna geometry (proposed antenna). (b) Modal magnitudes.

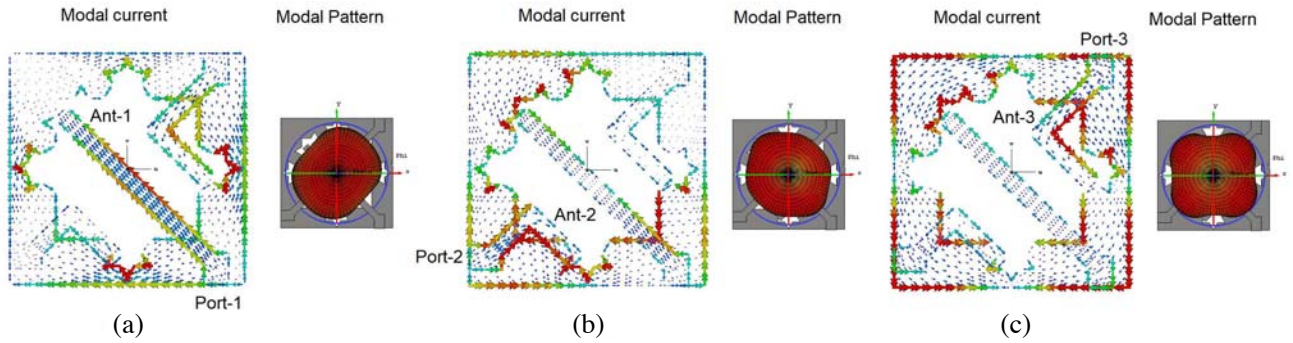

Figure 15. Modal currents and modal patterns. (a) Ant-1, (b) Ant-2, (c) Ant-3 configurations.

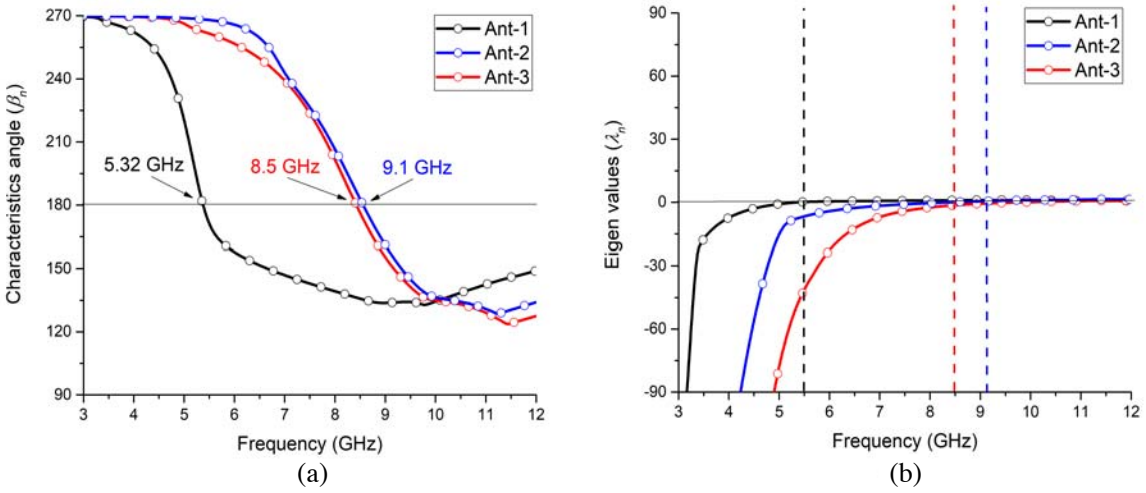

Figure 16. (a) Characteristics angle (β_n). (b) Eigen values (λ_n).

Table 1. Modal performance summary of proposed antenna geometries.

# Ant geometry	Ideal mode	B.W. potential	Q-factor	Radiative energy	Energy stored
Ant-1	Mode-1	UWB	Very low	Capacitive	Electric-field
Ant-2	Mode-2	Wideband	Moderately low	Capacitive	Electric-field
Ant-3	Mode-1	Wideband	Moderately low	Capacitive	Electric-field

4. 3-PORT MIMO ANTENNA DESIGN AND ANALYSIS

The proposed 3-port MIMO antenna geometry is shown in Figure 1, and fabricated prototype is shown in Figure 17. The antenna has a compact dimension of 28.6 mm × 28.6 mm and is fabricated on an FR-4 substrate (thickness = 1.6 mm, $\varepsilon_r = 4.3$, $\tan\delta = 0.02$). Initially, CMA investigation validates antenna performance, and now we extend our study on other numerical parameters. The simulated S-parameters (dB) and isolation parameters of each antenna element are shown in Figure 18. As stated earlier, Ant-1 operates in UWB mode and Ant-2/Ant-3 in wideband modes. The isolations are achieved, > 17 dB, when Ant-1 is excited, and Ant-2, Ant-3 are impedance matched with a 50 Ω load.

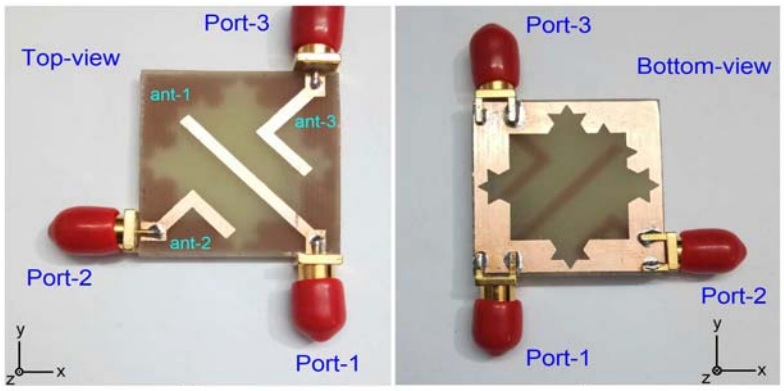

Figure 17. Fabricated prototype of proposed antenna with (a) top-view, (b) bottom-view.

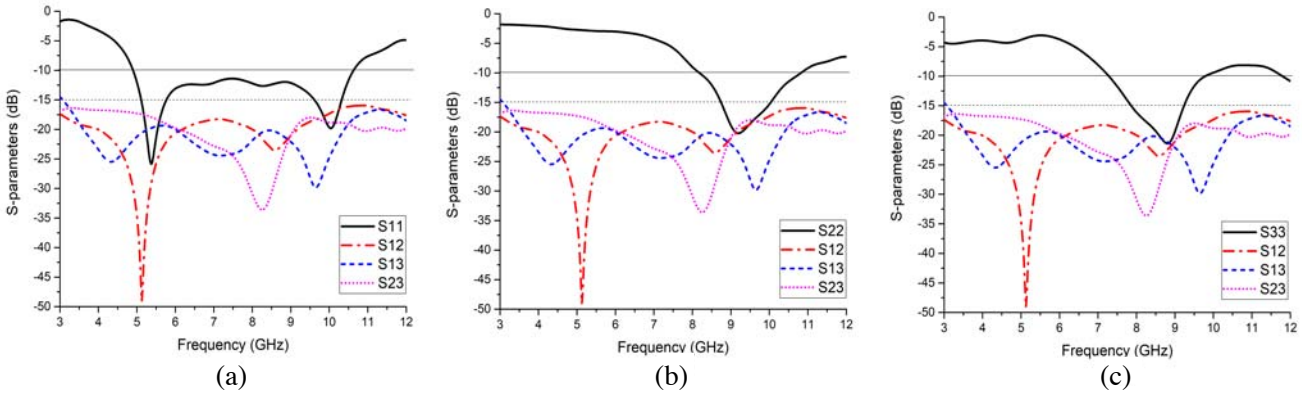

Figure 18. Simulated S-parameters of (a) Ant-1, (b) Ant-2, (c) Ant-3.

4.1. Geometry of Antenna and Ground Configuration

Ant-1 has 45° tilt configuration, and Ant-2, Ant-3 have mirror imaged L-shaped geometry. The deformity in structural configurations is made to enhance impedance characteristics specifically targeting cornered elements, i.e., Ant-2 and Ant-3 to be perfectly impedance matched. To further improve S_{11}-parameters, a Koch-fed fractal slot is etched in the ground plane (since fractal structure increases electrical length in a compact space). Initially, we have analyzed performances with full ground, square slot and fractal slot ground configurations shown in Figure 19(a). It is observed from the impedance responses shown in Figure 19(b) that fractal slot with ground has better matching response. Also the fractal slot acts as a perfect decoupler between antenna ports.

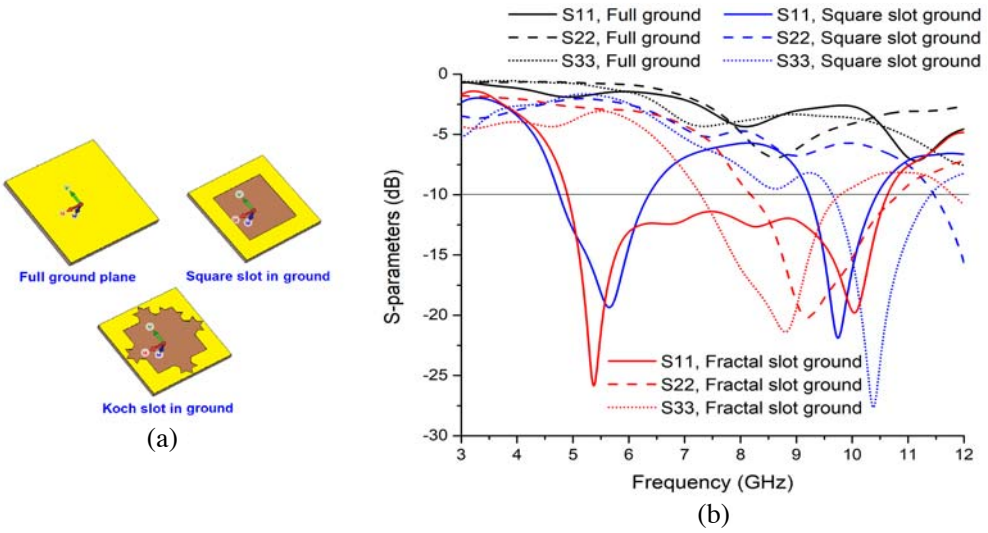

Figure 19. (a) Ground geometrical configurations. (b) S-parameter responses.

The isolation between antenna ports does not have any external decoupling network, which makes the prototype design compact. We have introduced fractal slot as a decoupler, since antenna excitation at each port has negligible coupling effect due to current diffractions. In order to investigate more on this isolation mechanism, surface current distributions at antenna elements are excited at corresponding resonant frequencies as shown in Figure 20. When Port-1 is excited at 5.32 GHz, maximum surface current exists only at Ant-1 and minimum surface currents observed at Port-2 and Port 3. When Port-2 is excited at 9.1 GHz, current maximum exists only at Ant-2, and current minima at Port-1 and Port 3.

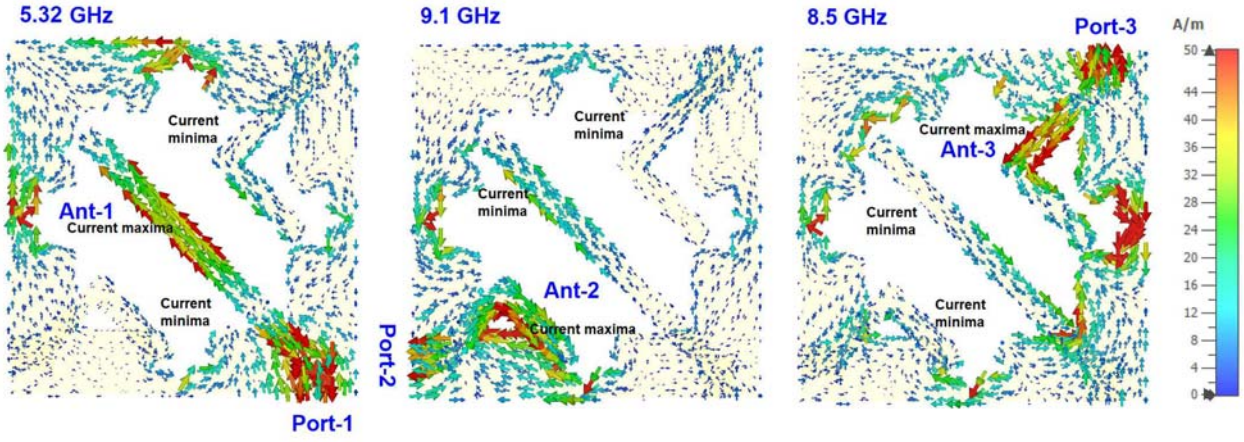

Figure 20. Surface current distributions at different frequencies excited at Ant-1, Ant-2 and Ant-3.

Similar effects are also observed for Port-3 at 8.5 GHz. The isolation parameters S_{12}, S_{23}, and S_{13} are > 17 dB in the operating bands. It is observed that slot decoupling strategy with antenna orientation has good port isolation with impedance matching characteristics in our proposed geometry.

5. RESULTS AND DISCUSSIONS

The proposed 3-port MIMO antenna is designed and simulated in CST MWS EM suite. A prototype is fabricated and measured in PNA series microwave network analyzer N5222A from Agilent Technologies.

The simulated and measured S-parameters are shown in Figure 21(a), and the isolation parameters are shown in Figure 21(b). The antenna S-parameters are measured when Port-1 is activated, and Port-2/Port-3 are matched terminated with 50 Ω load (similarly for Port-2 and Port-3). The antenna gains with efficiency for simulated and measured responses are shown in Figures 22(a) and 22(b), respectively. The reduction in efficiency is due to the presence of slot at ground and antenna clustering effect at top. The performances of proposed antenna are listed in Table 2. A discrepancy in varying results is due to substrate quality, dielectric effects, or connector soldering losses. To compute MIMO diversity parameters, envelope channel coefficient (ECC) is estimated from 3D complex far-field patterns

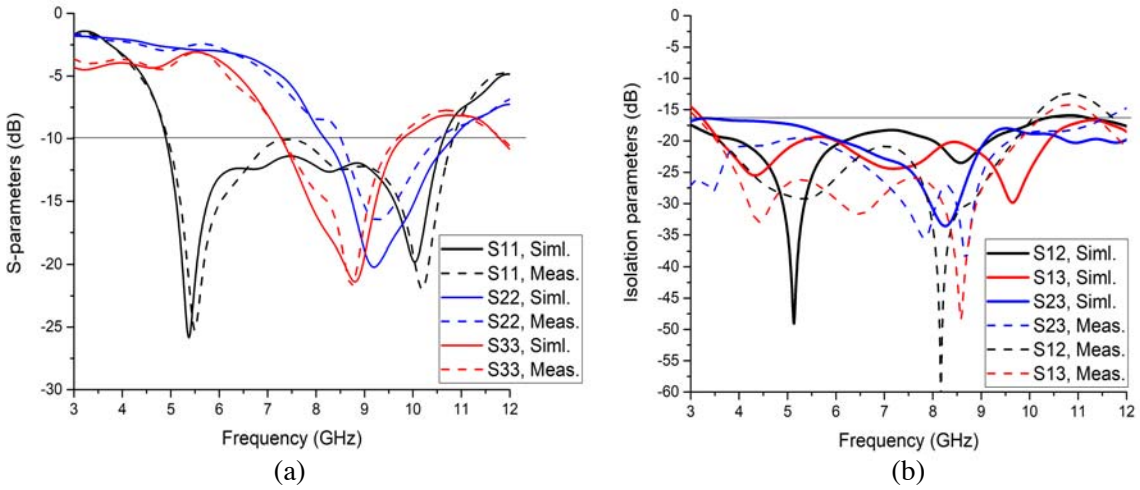

Figure 21. Simulated and measured results of (a) S-parameters, (b) isolation parameters of proposed 3-port MIMO antenna.

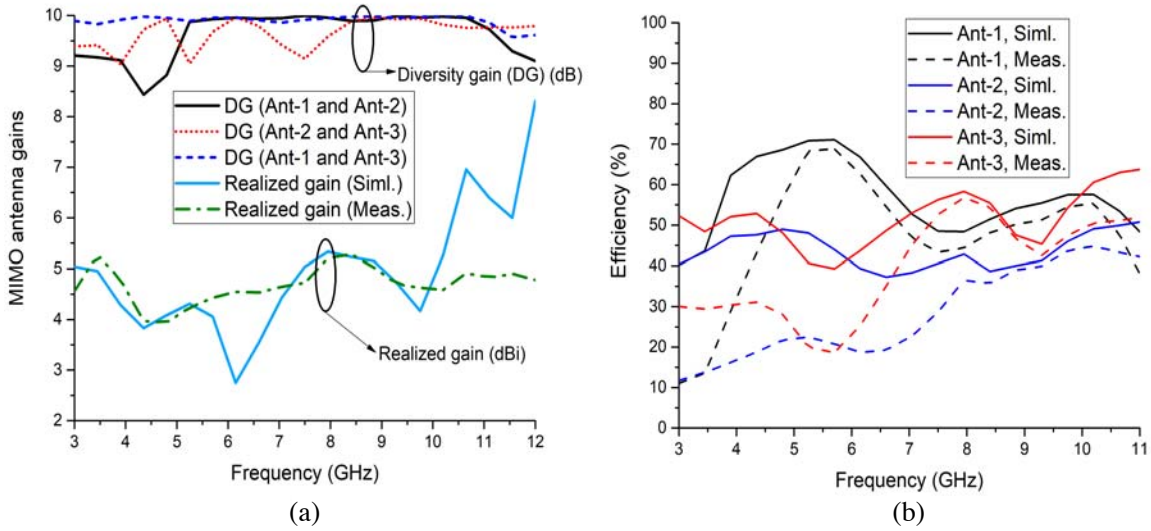

Figure 22. Simulated and measured results of (a) antenna gains, (b) efficiencies of 3-port MIMO antenna.

Table 2. Simulated and measured results summary of proposed 3-port MIMO antenna.

# Ant.	Siml./Meas. Frequency band	Siml./Meas. Isolation	Siml./Meas. Gain, Eff.	ECC
Ant-1	(4.8–10.6) GHz/(4.93–10.8) GHz	17 dB/16.9 dB	(3–7) dBi/(4–5.5) dBi, 70%/68%	0.022
Ant-2	(8.1–10.8) GHz/(8.5–10.5) GHz	20 dB/22 dB	4.7 dBi/4.5 dBi, 41%/40%	0.08
Ant-3	(7.2–9.8) GHz/(7.29–9.7) GHz	23.5 dB/26 dB	5.3 dBi/5.25 dBi, 46%/44%	0.03

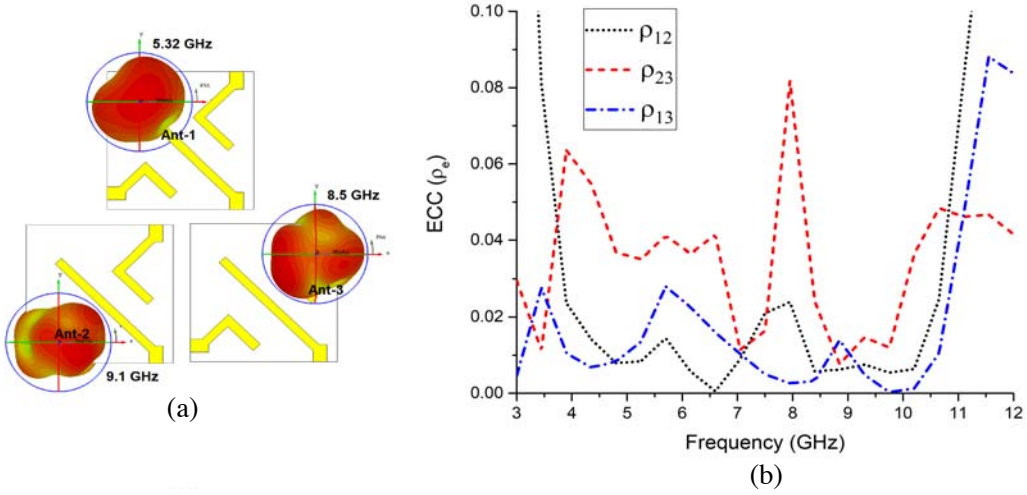

Figure 23. (a) 3D far-field patterns at each antenna element. (b) ECC of 3-port MIMO antenna.

collectively evaluated for Port-1, Port-2, and Port-3 captured field magnitudes for the best accuracy, considering an isotropic channel environment [23, 24]. From the ECC results, diversity gains [27] at each antenna ports is determined as: $\mathrm{DG} = \sqrt{1 - {\rho_e}^2}$ (where, ρ_e is the ECC at Port-1, Port-2, and Port-3).

Since 3-port MIMO antenna assists far-field pattern diversity due to large differentiation in radiative

patterns at each ports shown in Figure 23(a), the correlation factor between antenna elements is very low as observed from Figure 23(b). This effect can be best exploited for various MIMO applications with pattern diversity in a rich scattered environment and also confirms very low mutual-coupling between radiating elements in our proposed geometry.

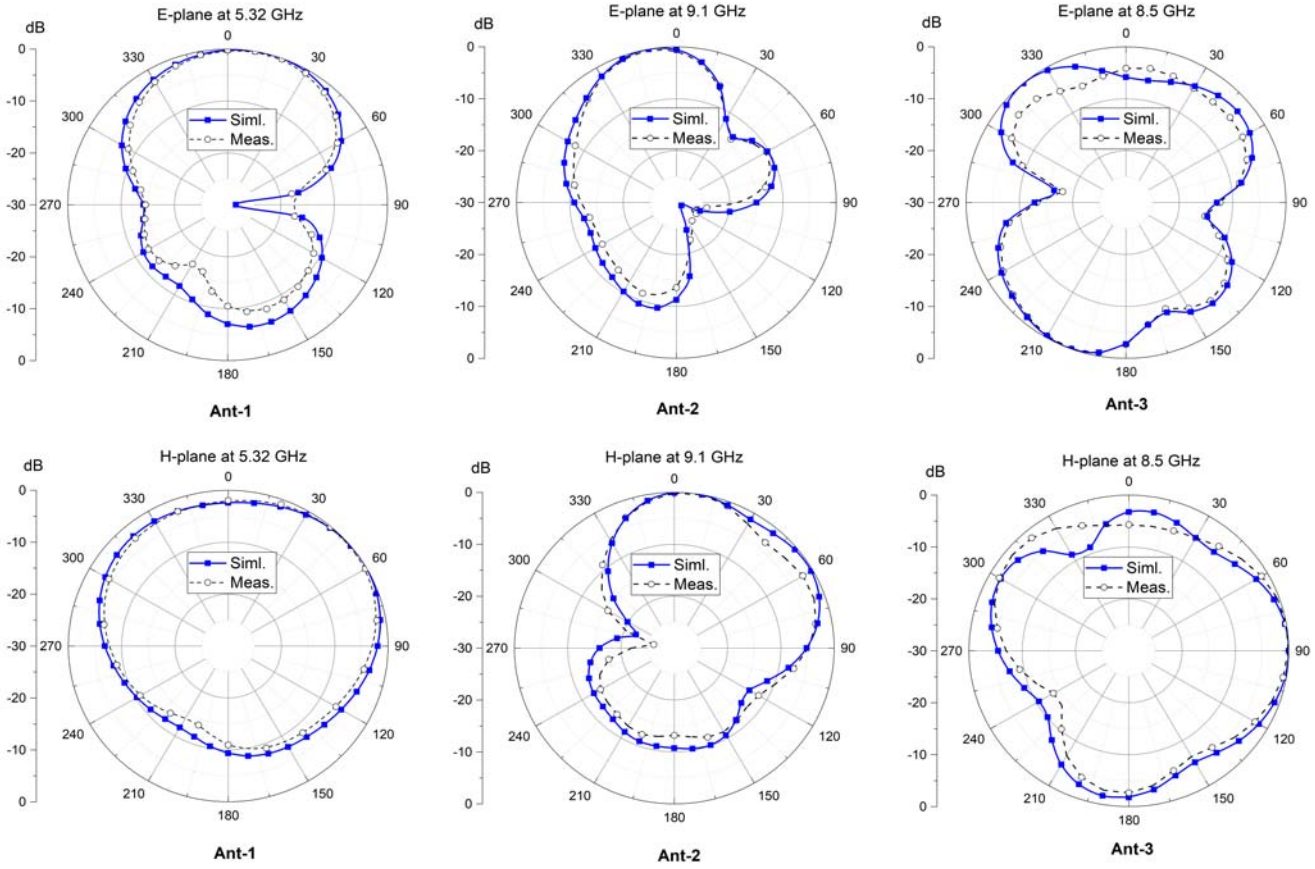

Figure 24. Simulated and measured radiation plots for Ant-1, Ant-2 and Ant-3 for proposed antenna.

Table 3. 3-port MIMO antenna performance comparision analysis.

Ref.	Ant. size	N_p	Port-isolation	Gain	Efficiency	Ant. design methodology
[10]	$0.053\lambda^2$	3	−15 dB	2.3 dBi	> 60%	Slots + (60°, 120°, 240° antenna orientations)
[12]	$0.519\lambda^2$	3	−18 dB	2.8–4.7 dBi	60–90%	Pattern diversity +Polarization diversity
[13]	$3.16\lambda^2$	3	−20 dB	7.4–8.1 dBi	-	DRA + 3 de-coupled mode excitations
[17]	$6.64\lambda^2$	3	−15 dB	5 dBi	70.3%	Integration of isolaton elements as radiators
This work	$0.208\lambda^2$	3	−17 dB	3–7 dBi	40–70%	Characteristics Mode Analysis

Note:- N_p = Number of ports used in antenna, λ = lowest operating wavelength

Figure 24 shows the simulated and measured radiation plots in E-plane and H-plane for Ant-1/2/3 (It is considered that when one port is active, all other ports are terminated with 50 Ω load). Di-pole like patterns exists in the E-plane, with radiation NULLS at $\pm 90^\circ$ and $+120^\circ$ due to antenna symmetry. Similarly, semi omni-like patterns are observed in the H-plane, but it shrinks in radiation strength due to Ant-2/3 reduced electrical size compared to Ant-1. There exists a differentiation in radiation patterns due to antenna orientation, hence pattern diversity is observed for all antenna elements. Due to high disclamation in the magnitudes of far-field strengths, low correlation between antennas is observed. The measured radiation plots slightly vary compared to simulated plots due to cabling effects during RF-power transmission in an anechoic chamber facility. The performance analyses of different 3-port MIMO antennas are compared in terms of electrical size, satisfactory port isolations, gain, radiation efficiency, and design methodology adopted to achieve different MIMO configurations, depicted in Table 3. To facilitate compact 3-port MIMO antenna design with diversity, a new topology has been adopted in our proposed work, which is successfully validated in both simulated and experimental environments. Also, the CMA adaptation reveals some important antenna parameters which can benefit in investigating numerical and analytical electromagnetic modelling of complex geometrical shapes and large antenna structures [28–35]. With CMA, the design analysis of large MIMO antenna arrays is also extended in massive MIMO applications.

6. CONCLUSION

This paper demonstrates a 3-port compact MIMO antenna assisting Characteristics Mode Analysis on different antenna geometries and ground structures. It reveals the ideal modes necessary for antenna resonance mechanism compared to other significant modes. The classical approach also analyzes antenna geometry to predict bandwidth potential, radiative energy source, and Q-factor. Finally, a prototype 3-port compact MIMO antenna is fabricated and measured, which is validated on good agreements for standard and MIMO performance metrics to be used for UWB, air traffic, defense tracking, meteorological, amateur satellite, maritime vessel traffic controlling, and X-band satellite applications.

REFERENCES

1. Shim, B. and B. Lee, "Evolution of MIMO technology," *The Journal of Korean Institute of Communications and Information Sciences*, Vol. 38, No. 8, 712–723, 2013.
2. Marzetta, T. L., "Massive MIMO: An introduction," *Bell Labs Technical Journal*, Vol. 20, No. 8, 11–22, 2015.
3. Mohammad, S. S., *Printed MIMO Antenna Engineering*, Artech House, 2014.
4. Jusoh, M., M. F. Bin Jamlos, M. R. Kamarudin, and M. F. Bin Abd Malek, "A MIMO antenna design challenges for UWB application," *Progress In Electromagnetics Research B*, Vol. 36, 357–371, 2012.
5. Sharawi, M. S., "Printed MIMO antenna systems: Performance metrics, implementations and challenges," *Forum for Electromagnetic Research Methods and Application Technologies (FERMAT)*, Vol. 1, 1–11, 2014.
6. Chiu, C.-Y., J.-B. Yan, and R. D. Murch, "Compact three-port orthogonally polarized MIMO antennas," *IEEE Antennas and Wireless Propagation Letters*, Vol. 6, 619–622, 2007.
7. Sarrazin, J., Y. Mahé, S. Avrillon, and S. Toutain, "Investigation on cavity/slot antennas for diversity and MIMO systems: The example of a three-port antenna," *IEEE Antennas and Wireless Propagation Letters*, Vol. 7, 414–417, 2008.
8. Kotb, I. E., R. S. Ghoname, H. H. Ghoz, and H. Kaldass, "Three port MIMO antenna for 4G application," *International Journal of Advancements in Research & Technology*, Vol. 1, No. 4, 1–3, 2012.
9. Wang, H., L. Liu, Z. Zhang, and Z. Feng, "Wideband tri-port MIMO antenna with compact size and directional radiation pattern," *Electronics Letters*, Vol. 50, No. 18, 1261–1262, 2014.

10. Wang, H., L. Liu, Z. Zhang, Y. Li, and Z. Feng, "Ultra-compact three-port MIMO antenna with high isolation and directional radiation patterns," *IEEE Antennas and Wireless Propagation Letters*, Vol. 13, 1545–1548, 2014.
11. Bahramzy, P., S. Svendsen, and G. F. Pedersen, "Isolation between three antennas at 700 MHz: For handheld terminals," *IET Microwaves, Antennas and Propagation*, Vol. 9, No. 3, 237–242, 2014.
12. Sharma, Y., D. Sarkar, K. Saurav, and K. V. Srivastava, "Three-element MIMO antenna system with pattern and polarization diversity for WLAN applications," *IEEE Antennas and Wireless Propagation Letters*, Vol. 16, 1163–1166, 2016.
13. Abdalrazik, A., A. S. Abd El-Hameed, and A. B. Abdel-Rahman, "A three-port MIMO dielectric resonator antenna using decoupled modes," *IEEE Antennas and Wireless Propagation Letters*, Vol. 16, 3104–3107, 2017.
14. Deng, J.-Y., J.-Y. Li, and L.-X. Guo, "Decoupling of a three-port MIMO antenna with different impedances using reactively loaded dummy elements," *IEEE Antennas and Wireless Propagation Letters*, Vol. 17, No. 3, 430–433, 2018.
15. Saurav, K., N. K. Mallat, and Y. M. M. Antar, "A three-port polarization and pattern diversity ring antenna," *IEEE Antennas and Wireless Propagation Letters*, Vol. 17, No. 7, 1324–1328, 2018.
16. Swapna, S. P., G. S. Karthikeya, S. K. Koul, and A. Basu, "Three-port pattern diversity antenna module for 5.2 GHz ceiling-mounted WLAN access points," *Progress In Electromagnetics Research C*, Vol. 98, 57–67, 2020.
17. Chen, W.-S. and R.-D. Lin, "Three-port MIMO antennas for laptop computers using an isolation element as a radiator," *International Journal of RF and Microwave Computer-Aided Engineering*, 2020.
18. Garbacz, R. J., "Modal expansions for resonance scattering phenomena," *Proceedings of the IEEE*, Vol. 53, No. 8, 856–864, 1965.
19. Harrington, R. and J. Mautz, "Theory of characteristic modes for conducting bodies," *IEEE Transactions on Antennas and Propagation*, Vol. 19, No. 5, 622–628, 1971.
20. Mohanty, A. and B. R. Behera, "Investigation of 2-port UWB MIMO diversity antenna design using characteristics mode analysis," *AEU-International Journal of Electronics and Communications*, Vol. 124, No. 5, 153361, 2020.
21. Zhao, X., S. P. Yeo, and L. C. Ong, "Planar UWB MIMO antenna with pattern diversity and isolation improvement for mobile platform based on the theory of characteristic modes," *IEEE Transactions on Antennas and Propagation*, Vol. 66, No. 1, 420–425, 2017.
22. Perli, B. R. and A. M. Rao, "Characteristic mode analysis of wideband microstrip antenna," *Progress In Electromagnetics Research C*, Vol. 97, 201–212, 2019.
23. Elshirkasi, A. M., A. Abdullah Al-Hadi, M. F. Mansor, R. Khan, and P. J. Soh, "Envelope correlation coefficient of a two-port MIMO terminal antenna under uniform and Gaussian angular power spectrum with user's hand effect," *Progress In Electromagnetics Research C*, Vol. 92, 123–136, 2019.
24. Kildal, P.-S. and K. Rosengren, "Correlation and capacity of MIMO systems and mutual coupling, radiation efficiency, and diversity gain of their antennas: Simulations and measurements in a reverberation chamber," *IEEE Communications Magazine*, Vol. 42, No. 12, 104–112, 2004.
25. Anguera, J., J.-P. Daniel, C. Borja, J. Mumbru, C. Puente, T. Leduc, N. Laeveren, and P. van Roy, "Metallized foams for fractal-shaped microstrip antennas," *IEEE Antennas and Propagation Magazine*, Vol. 50, No. 6, 20–37, 2008.
26. Anguera, J., C. Puente, C. Borja, and J. Soler, "Fractal shaped antennas: A review," *Wiley Encyclopedia of RF and Microwave Engineering*, edited by K. Chang, Vol. 2, 1620–1635, 2005.
27. Mohanty, A. and S. Sahu, "High isolation two-port compact MIMO fractal antenna with Wi-Max and X-band suppression characteristics," *International Journal of RF and Microwave Computer-Aided Engineering*, Vol. 30, No. 1, e22021, 2020.
28. Valagiannopoulos, C., "On measuring the permittivity tensor of an anisotropic material from the transmission coefficients," *Progress In Electromagnetics Research B*, Vol. 9, 105–116, 2008.

29. Zhou, T., T. Hu, and Z. Ge, "Dispersive rayleigh wave attenuation using inverse-dispersion method," *ASEG Extended Abstracts*, 1–4, 2010.
30. Tagay, Z. and C. Valagiannopoulos, "Highly selective transmission and absorption from metasurfaces of periodically corrugated cylindrical particles," *Phys. Rev. B*, Vol. 98, No. 11, 115306, 10 Pages, 2018.
31. Siddiqui, O. F. and A. S. Mohra, "Microwave dielectric sensing in hyperbolically dispersive media," *IEEE Sensors Letters*, Vol. 1, No. 6, 1–4, 2017.
32. Valagiannopoulos, C. A. and S. A. Tretyakov, "Symmetric absorbers realized as gratings of PEC cylinders covered by ordinary dielectrics," *IEEE Transactions on Antennas and Propagation*, Vol. 62, No. 10, 5089–5098, 2014.
33. Alitalo, P., C. A. Valagiannopoulos, and S. A. Tretyakov, "Simple cloak for antenna blockage reduction," *2011 IEEE International Symposium on Antennas and Propagation (APSURSI)*, 669–672, Spokane, WA, USA, 2011.
34. Chen, L., X. Ren, Y.-Z. Yin, and Z. Wang, "Broadband CPW-fed circularly polarized antenna with an irregular slot for 2.45 GHz RFID reader," *Progress In Electromagnetics Research Letters*, Vol. 41, 77–86, 2013.
35. Valagiannopoulos, C., "Single-series solution to the radiation of loop antenna in the presence of a conducting sphere," *Progress In Electromagnetics Research*, Vol. 71, 277–294, 2007.